ADVANCED PHYSICS RESEARCH Open Access
www.advphysicsres.com

Transition Characteristics of Non-Hermitian Skin Effects in a Zigzag Lattice Without Chiral Symmetry

Xiaoxiong Wu, Luojia Wang, Shihua Chen,* Xianfeng Chen, and Luqi Yuan**

Non-Hermitian systems recently have attracted tremendous attention due to their plentiful unique and fascinating properties, among which is the localization of an otherwise extensive bulk eigen-state at the boundary when the open boundary condition (OBC) is imposed, an interesting phenomenon now referred to as non-Hermitian skin effect (NHSE). Here, a non-Hermitian Zigzag lattice model with/without chiral symmetry is investigated with respect to different nearest-neighbor and long-range hopping amplitudes and study the transition signature of NHSE by extracting information from the complex eigen-energy spectra of the system under the periodic boundary condition (PBC), which is verified by the directional inverse participation ratio under OBC. Such an approach provides great simplicity in judging transitions of NHSE especially in lattices without chiral symmetry, where the obtained transition signatures are further confirmed by calculating the topological winding number of the energy under PBC. This work reveals a fundamental way to explore transitions of NHSE, and has a potential in helping understand more other complicated topological physics unique to non-Hermitian systems.

1. Introduction

In quantum mechanics, physical observables are linked to Hermitian Hamiltonian, which describes isolated quantum systems and enables the eigen-energy to be one-to-one correspondence between open boundary condition (OBC) and periodic boundary condition (PBC) except for the topological edge states that may appear at the open ends.[1–6] This Bloch band theory provides an essential approach to predicting the topological phase of classical/quantum systems. However, many physical systems hold energy exchange from the ambient environment, and some may even exhibit asymmetrical spatial couplings, rendering the intrinsic Hamiltonian non-Hermitian.[7–12] Interestingly, different from conventional Hermitian system, non-Hermitian system, either classical or quantum, has recently become an emergent research front and has attracted rapidly growing interest in past decades,[13–32] which shows abundant characteristics in its complex energy bands and thereby brings about many novel physical phenomena seen in broad physical settings such as optical crystals,[32–35] mechanical lattices,[36–38] electric circuits,[39–42] acoustic systems,[43–46] and many others.[47–49]

The eigen-energy of a non-Hermitian Hamiltonian is usually complex, but it has been found that the system with parity-time symmetry can support pure real eigen-energy spectra,[4,7,47,50–53] which triggers an explosion of research in photonics[27,54–58] and entails fruitful intriguing properties such as mode switching,[59,60] unidirectional invisibility,[7,61,62] and chiral damping/amplification.[63–65] Nevertheless, most non-Hermitian systems still have complex eigen-energy, and only very recently did researchers find the non-Hermitian skin effect (NHSE), which is now identified as one of the most prominent phenomena in non-Hermitian systems.[18–21] It turns out that bulk modes could transform into analogous boundary states, that is, anomalous localizations, by which we mean that distributions of the corresponding bulk eigen-states exponentially pile up and get squeezed toward one of the boundaries under OBC.[66–68] Such an exotic phenomenon seems to manifest a breakdown of the conventional bulk-boundary correspondence that works well for the Hermitian Bloch Hamiltonian.[18,19,69–72] To better understand NHSE and then predict the existence of NHSE in a given physical model, researchers have proposed to utilize the general Brillouin zone (GBZ)[19–21,73] to efficiently criticize the bulk localization feature, yet the process to calculate the GBZ is quite complicated in spite of subsequent improved auxiliary GBZ

X. Wu, L. Wang, X. Chen, L. Yuan
State Key Laboratory of Advanced Optical Communication Systems and Networks
School of Physics and Astronomy
Shanghai Jiao Tong University
Shanghai 200240, China
E-mail: ljwang@sjtu.edu.cn; yuanluqi@sjtu.edu.cn
S. Chen
School of Physics and Frontiers Science Center for Mobile Information Communication and Security
Southeast University
Nanjing 211189, China
E-mail: cshua@seu.edu.cn

The ORCID identification number(s) for the author(s) of this article can be found under https://doi.org/10.1002/apxr.202300007

DOI: 10.1002/apxr.202300007

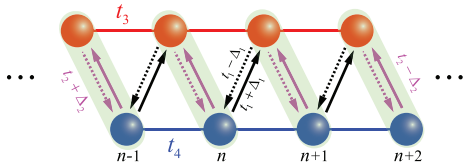

Figure 1. Schematic of the Zigzag lattice model with nonreciprocal hopping amplitudes between different sublattice sites. The green box indicates a unit cell where the sites are in red and blue, respectively. $t_{1,2} \pm \Delta_{1,2}$ are real nearest-neighbor hopping amplitudes, where $\Delta_{1,2}$ denote the coupling offsets on the corresponding hoppings that will contribute to the non-Hermiticity. $t_{3,4} \in R$ represent the long-range (next-nearest-neighbor) hopping amplitudes.

method.[25] This complexity usually becomes more evident if the system does not possess a chiral symmetry. Now a natural question arises as to whether one can capture some characteristics from the eigen-energy spectra problem in lattices without chiral symmetry, and how to apply them to predict transitions of NHSE.

In this paper, we study the transition characteristics of NHSE in a non-Hermitian Zigzag lattice model that can hold no chiral symmetry under conditions of a judicious choice of parameters. A new correspondence relationship between PBC and OBC is established by exploring the eigen-energy spectra under PBC and the directional inverse participation ratio (dIPR) under OBC. We find that the transitions of NHSE are closely linked to the real parts of eigen-energy spectra, which has been further confirmed to be consistent with the results calculated from the winding number and GBZ. Our work brings new thoughts into the study of the relationships between NHSE and eigen-energy spectra, which can be extended into a broader range of non-Hermitian models for predicting NHSE phenomena, thereby providing new avenues for understanding the elusive non-Hermitian physics in different systems.

The rest of this paper is organized as follows. In Section 2, we start by introducing our 1D lattice model and the related Hamiltonian. In Section 3, we analyze the localization characteristics of NHSE in lattices without long-range hopping amplitudes. We further include single and double long-range hopping amplitudes, and explore the transition characteristics of NHSE in detail for specific sets of parameters in Section 4 and 5, respectively. We give a brief summary in Section 6.

2. Models

We consider a 1D tight-binding lattice including two sublattices A and B per unit cell as shown in **Figure 1**. Such two sublattices are staggered with two columns of 1D lattices, equivalent to a 1D non-Hermitian *Su-Schrieffer-Heeger* (SSH) model[74,75] with reciprocal long-range hopping amplitudes. The corresponding Hamiltonian under the OBC is

$$\begin{aligned} H = &\sum_{n=1}^{N} \left[(t_2+\Delta_2)b_n^\dagger a_n + (t_2-\Delta_2)a_n^\dagger b_n\right] \\ &+ \sum_{n=1}^{N-1} \left[(t_1+\Delta_1)a_{n+1}^\dagger b_n + (t_1-\Delta_1)b_n^\dagger a_{n+1}\right. \\ &\left. + t_3(a_n^\dagger a_{n+1} + a_{n+1}^\dagger a_n) + t_4(b_n^\dagger b_{n+1} + b_{n+1}^\dagger b_n)\right] \end{aligned} \tag{1}$$

where $a_n^\dagger(b_n^\dagger)$ and $a_n(b_n)$ are creation and annihilation operators of the bosonic excitation on sublattice A (B) in the n-th unit cell. $t_{1,2,3,4} \in R$ are real hopping amplitudes and $\Delta_{1,2}$ are the coupling offsets on the corresponding hoppings in the lattice in Figure 1. Note that all parameters $t_{1,2,3,4}$ and $\Delta_{1,2}$ are taken the same frequency unit with $\hbar$=1, so the Hamiltonian is scalable and in what follows, we will set these parameters to be dimensionless for simplicity. Under this design, one can see that the nearest-neighbor hoppings between sublattices A and B are asymmetric or nonreciprocal, which are the origin of non-Hermiticity of Hamiltonian (1), while the next-nearest-neighbor hoppings between two sublattices A (or B) are reciprocal.

3. Study Models Without Long-Range Hopping Amplitudes

We start from analyzing the lattice in Figure 1 without the long-range hopping amplitudes t_3 and t_4. First, let us consider the case for an infinitely extended lattice under PBC. Performing the Fourier transformation, one can obtain the Hamiltonian in the momentum (k) space as

$$\begin{aligned} \mathcal{H}(k) &= \begin{bmatrix} 0 & (t_1+\Delta_1)e^{-ik} + (t_2-\Delta_2) \\ (t_1-\Delta_1)e^{ik} + (t_2+\Delta_2) & 0 \end{bmatrix} \\ &= \begin{bmatrix} 0 & h_x - ih_y \\ h_x + ih_y & 0 \end{bmatrix} = h_x\sigma_x + h_y\sigma_y \end{aligned} \tag{2}$$

where $\sigma_{x,y}$ are the Pauli matrices and $h_x = t_2 + t_1\cos k - i\Delta_1 \sin k$, $h_y = t_1 \sin k + i(\Delta_1 \cos k - \epsilon_2)$. The Hamiltonian in Equation 2 is non-Hermitian and satisfies the chiral symmetry, that is, $\sigma_z\mathcal{H}(k)\sigma_z = -\mathcal{H}(k)$. From the Hamiltonian (2), the eigen-energy spectra keep symmetrical under PBC for k in the entire first Brillouin zone (BZ) $0 \leqslant k < 2\pi$, which hold the following expressions:

$$\begin{aligned} E_\pm(k) &= \pm\sqrt{h_x^2 + h_y^2} \\ &= \pm\sqrt{\begin{aligned} &t_1^2 + t_2^2 - (\Delta_1{}^2 + \Delta_2{}^2) + 2(t_1t_2 + \Delta_1\Delta_2)\cos k \\ &- i2(t_1\Delta_2 + \Delta_1 t_2)\sin k \end{aligned}} \end{aligned} \tag{3}$$

3.1. Model with $\Delta_2 = 0$

We first consider the examples with parameters $t_2 = 1$, $\Delta_1 = 0.5$, and $\Delta_2 = 0$ but let t_1 be tunable. We set $t_1 = 2$, and plot the eigen-energy spectra for k from 0 to 2π in the first BZ in **Figure 2**a. The arrows denote dynamical evolution for the spectra under PBC, so one can see that two closed curves evolve clockwise with k increasing from 0 to 2π in the complex energy plane.

Now, we study the same lattice but under OBC, by taking N = 100 in the Hamiltonian Equation 1 with other parameters being kept unchanged. The resultant energy spectra are plotted in Figure 2a, with the corresponding distributions of eigen-modes shown in Figure 2b. We notice that the eigen-energy spectra under OBC are embraced within the ones under PBC except for a pair of zero modes corresponding to the degenerate zero energy

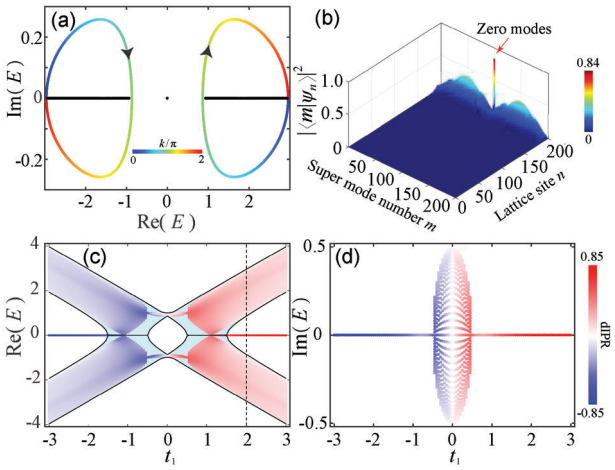

Figure 2. a) The eigen-energy spectra under PBC (multi-colored dots) and OBC (black dots) at the black dashed line $t_1 = 2$ in (c), showing the winding behavior of $E(k)$ for $k \in [0, 2\pi)$. b) The calculated eigen-mode distributions of (a) under OBC for the lattice with $N = 100$. c,d) The real and imaginary parts of the OBC spectra as a function of $t_1 \in [-3, 3]$, where the colored data point represents dIPR. The cyan regime with the black lines in (c) shows the real parts of the eigen-energy spectra under PBC. The other parameters are chosen to be $t_2 = 1$, $t_3 = t_4 = 0$, $\Delta_1 = 0.5$ and $\Delta_2 = 0$.

in the eigen-energy spectra and are closely linked to the projections of the spectra under PBC onto the real axis, which shows the connection between the eigen-energy spectra under PBC and those under OBC in our model.

Here, the distributions of eigen-modes in Figure 2b reveal localization features, that is, NHSE. In this figure, the bulk states are localized at the right boundary, together with a pair of zero modes. We define the inverse participation ratio (IPR)[69,76,77] for quantitative judgment of the mode distribution:

$$\mathrm{IPR}(\psi_m) = \sum_{j=1}^{2N} \frac{\left|\psi_{m,j}\right|^4}{\left(\langle\psi_m|\psi_m\rangle\right)^2} \tag{4}$$

where $\psi_{m,j}$ is the j-th component (i.e., j is odd for lattice A and even for lattice B) for the eigen-state ψ_m satisfying the Schrödinger equation $H|\psi_m\rangle = E_m|\psi_m\rangle$, and E_m is the m-th eigen-energy. IPR approaches to 1 for a localized state but to 0 for an extended state. To further distinguish the left or right localization feature, we use the directional IPR (dIPR):[76]

$$\begin{cases} \mathrm{dIPR}(\psi_m) = P\left(\psi_m\right)\mathrm{IPR}\left(\psi_m\right), \\ P\left(\psi_m\right) = \mathrm{sgn}\left[\sum_{j=1}^{2N}\left(j - N - 0.5\right)\left|\psi_{m,j}\right|\right] \end{cases} \tag{5}$$

Therefore, in our cases, the distributions of eigen-modes (ψ_m) would be entirely localized at the right boundary when dIPR→+1, and at the left boundary when dIPR→ −1, while they become fully extended when dIPR→0.

With dIPR defined, we here present the eigen-energy spectra variation with the parameter t_1 from −3 to 3 and show the change of dIPR on the spectra in Figure 2c,d. We also compare the real part of the spectra with the real energy projections in the case under PBC (see the cyan regime surrounded by black lines in Figure 2c). One can see that, with t_1 increasing, the bulk states change from the left-localized NHSE to the right-localized one, and the spectra transition plots display a well-symmetrical performance due to the chiral symmetry under OBC, that is, $\Gamma H \Gamma^{-1} = -H$ with $\Gamma = diag(1, -1, 1, -1, ..., 1, -1)$, which means that $\Gamma|\psi_m\rangle$ also is an eigen-mode of the eigen-energy $-E_m$.

We see that $t_1 = 0$ is the transition point of NHSE where the real eigen-energy spectra under PBC shrink to their narrowest ranges, as shown in Figure 2c. When inspecting them in the complex energy plane, the PBC energy spectra at this transition point would trace back and forth along an open curve, or along a closed curve with no interior space. On the other hand, in previous studies, to see the transition signature of NHSE under the change of parameters, one often resorts to certain criteria such as topological winding number which are proved to be effective but generally involve complicated calculations. For example, the topological winding number[78,79] depicting the localization feature of NHSE is given by

$$w(E) = \oint_{BZ} \frac{1}{2\pi i} \frac{d\left[\ln\det\left(\mathcal{H}(k) - E\right)\right]}{dk} dk \tag{6}$$

where E is the base energy and $w(E)$ gives the number of encirclement of the complex energy spectra under PBC around this base energy E as k runs along the BZ by associating its positive value (clockwise rotation) and negative value (counterclockwise rotation) to the right and left localized NHSEs, respectively. Naturally, if $w(E) = 0$, then it corresponds to a conventional bulk mode without any NHSE. For example, in the case of Figure 2, when $t_1 > 0$, the distributions of NHSE localize at the right boundary of the lattice resulting in $w > 0$, which corresponds to the clockwise winding of the eigen-energy spectra, as one can see in Figure 2a. When $t_1 < 0$, the contrary would be the case. One may note that, although $w(E)$ is extremely useful in judging the transition of NHSE, the calculation involving line integration in the complex plane is quite cumbersome and thus less efficient.

Meanwhile, from the physical aspect, the localized property of NHSE also represents the appearance of the persistent current, $I = \int_0^{2\pi} f(E, E^*)E'(k)dk = \oint_{\mathrm{BZ}} \mathrm{Im}(E)\, d\mathrm{Re}(E)$ where f is a distribution function defined as $f(E, E^*) = \frac{E - E^*}{2i} = \mathrm{Im}(E)$ in the complex energy plane and $E'(k)$ represents a differential for the interior space of closed eigen-energy spectra under PBC.[73] Here, again $\lim_{t_1 \to 0} I \approx 0$ corresponds to the transition point of NHSE. This approach includes an integration expressing the area circling total eigen-energy spectra, so it puts a demand on the differential term to ensure accuracy. All above analysis methods are consistent with each other, and confirm the transition characteristics of NHSE that can be seen directly from the real eigen-energy spectra under PBC together with the dIPR under OBC in Figure 2c.

3.2. Model with $\Delta_2 \neq 0$

We now consider the case with $\Delta_2 = 0.5$ which therefore makes the lattice spatially non-reciprocal, and plot the eigen-energy spectra with dIPR in **Figure 3**a,b. Although the extra coupling

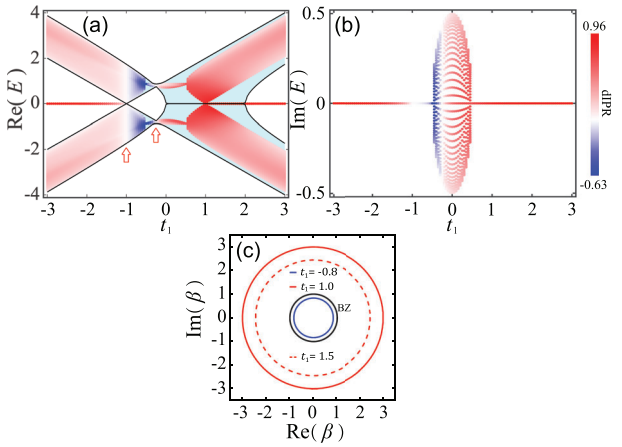

Figure 3. a,b) The real and imaginary parts of eigen-energy spectra under OBC as a function of $t_1 \in [-3, 3]$ in models including double nonreciprocal coupling amplitudes. The cyan regime with the black lines labels the real eigen-energy spectra under PBC in (a). The arrows indicate two transitions where dIPR=0 in white under OBC. c) The GBZs under OBC for the lattice with $N = 41$ at $t_1 = -0.8$ and 1.0, respectively, where the black one is a unit circle. The parameters are chosen to be $t_2 = 1$, $t_3 = t_4 = 0$, $\Delta_1 = 0.5$ and $\Delta_2 = 0.5$.

offset Δ_2 does not induce obvious eigen-energy deviations under OBC if one compares Figure 3a,b with Figure 2c,d, the dIPR distributions exhibit a distinct difference. More interestingly, for spectra with $t_1 > 0$ in Figure 3a, there exists a black solid line around Re(E)=0 that separates upper and lower spectra under PBC, which is generated from $\min\{E_+\} = \max\{E_-\} = E_+(\pi) = E_-(\pi)$ in Equation 3 with the eigen-energy spectra turning into a closed curve from end to end in the entire BZ of $k \in [0, 2\pi)$.

In Figure 3a, it is clear to see that two transitions occur in contrast with the result of the previous case in Figure 2, that is, one at $t_1 = -1$ while the other at $t_1 = -0.25$. One can understand such transitions from Equation 3 explicitly. As $t_1 = -\Delta_1 t_2/\Delta_2 = -1$, the eigen-energy spectra under PBC centralize in the real axis and overlap with the ones under OBC and the imaginary part of spectra (Im[$E(k)$]) is 0 for all k's. The other transition comes up at $\Delta E_R \equiv \mathrm{Re}[E(k=0)] - \mathrm{Re}[E(k=\pi)] = 0$, that is, the width of real spectra being zero at $t_1 = -0.25$ in Figure 3a. These characteristics not only reflect richer features of the eigen-energy spectra in contrast with Figure 2 but also manifest that the transitions can be predicted by spectra under PBC together with dIPR under OBC.

To further verify such transitions here, we calculate the GBZs to demonstrate localization features under OBC.[18,20,21,73] We follow the standard approach and substitute k into the general Bloch wave number $e^{ik} \to \beta$, and obtain the non-Bloch Hamiltonian $H(\beta) = R_+(\beta)\sigma_+ + R_-(\beta)\sigma_-$ from Equation 2, where $\sigma_\pm = (\sigma_x \pm i\sigma_y)/2$, and

$$\begin{cases} R_+(\beta) = (t_1 + \Delta_1)\beta^{-1} + (t_2 - \Delta_2), \\ R_-(\beta) = (t_1 - \Delta_1)\beta + (t_2 + \Delta_2) \end{cases} \tag{7}$$

Now, the eigen-energy equation takes the form

$$\left[(t_1 + \Delta_1)\beta^{-1} + (t_2 - \Delta_2)\right]\left[(t_1 - \Delta_1)\beta + (t_2 + \Delta_2)\right] = E^2 \tag{8}$$

This quadratic equation has two solutions β_1 and β_2 which form the GBZ for given t_1. We here choose $t_1 = -0.8$, 1.0, 1.5, respectively, and calculate the corresponding GBZs, with results shown in Figure 3c. One can see that for $t_1 = 1.0$, 1.5(− 0.8), the GBZ is outside (inside) the unit circle, indicating that the bulk modes display the right (left) localization features, which are consistent with the dIPR distributions. We can analytically calculate the transition point by calculating Equation 8 and get $|\beta| = \sqrt{|\frac{(t_1+\Delta_1)(t_2+\Delta_2)}{(t_1-\Delta_1)(t_2-\Delta_2)}|}$ by using the Schrödinger equation with finite lattices,

$$\begin{cases} (t_1 + \Delta_1)\psi_{m-1,B} + (t_2 - \Delta_2)\psi_{m,B} = E\psi_{m,A}, \\ (t_2 + \Delta_2)\psi_{m,A} + (t_1 - \Delta_1)\psi_{m+1,A} = E\psi_{m,B} \end{cases} \tag{9}$$

and find the transitions appearing at $|\beta| = 1$, namely, when the GBZ coincides with BZ circle.[19,20] This procedure results in two final equations $t_1\Delta_2 + \Delta_1 t_2 = 0$ and $t_1 t_2 + \Delta_1\Delta_2 = 0$. Therefore, for the case in Figure 2, the solution gives the transition at $t_1 = 0$, while for the case in Figure 3, solutions give transitions at $t_1 = -1.0$ and -0.25.

In these two examples, we see differences between two models with reciprocal and non-reciprocal hopping amplitudes. The transitions of NHSE can be obtained from the real eign-energy spectra under PBC combined with dIPR under OBC. Such transitions are verified by other approaches including the GBZ, winding number, and visual mode distribution. However, we can see, as well as from more complicated examples in the later sections, that information from spectra itself provides a simpler way to predict transitions.

4. Study Model with Single Long-Range Hopping Amplitudes

Now, we study the same lattice model in Figure 2 but with $t_3 \neq 0$, which makes the lattice model break the chiral symmetry. The Hamiltonian Equation 2 becomes

$$\mathcal{H}(k) = \begin{bmatrix} 2t_3\cos k & (t_1 + \Delta_1)e^{-ik} + (t_2 - \Delta_2) \\ (t_1 - \Delta_1)e^{ik} + (t_2 + \Delta_2) & 0 \end{bmatrix} \tag{10}$$

which includes a non-zero diagonal term. We plot the eigen-energy spectra in **Figure 4**, which exhibits asymmetrical feature in positive and negative t_1 regimes. We still can capture the transitions of NHSE from the eigen-energy spectra in Figure 4a–c. For the upper spectra, the transition occurs at $t_1 = -0.57$ when the closed eigen-energy spectra under PBC have no interior. One notes that such minimum width of real spectra ΔE_R corresponds to the conversion of the direction for the eigen-energy winding along $k \in [0, 2\pi)$ under PBC. The imaginary part of eigen-energies and corresponding dIPR distributions for the upper spectra in Figure 4c reflect such transition features. A similar transition at $t_1 = 0.57$ can also be seen from the lower spectra. Thus, the real spectra directly exhibit the transitions of NHSE, which is in consistent with dIPR distributions as shown in Figure 4a–c.

To further understand these localized properties of NHSE at different regimes, we choose $t_1 = 0.2$ and 1.0, respectively and

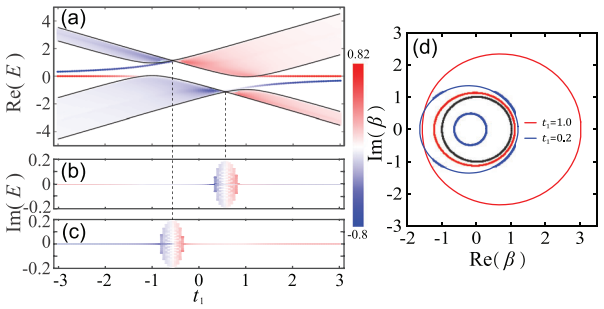

Figure 4. a–c) The real and imaginary parts of eigen-energy spectra under OBC as a function of $t_1 \in [-3, 3]$ in models including single long-range hopping amplitudes. The cyan regime with the black lines labels the real eigen-energy spectra under PBC in (a). The black dashed lines are two transitions where dIPR=0 in white under OBC. d) The GBZs under OBC for the lattice with $N = 41$ at $t_1 = 0.2$ and 1.0. The parameters are chosen to be $t_2 = 1$, $t_3 = 0.5$, $t_4 = 0$, $\Delta_1 = 0.2$ and $\Delta_2 = 0$.

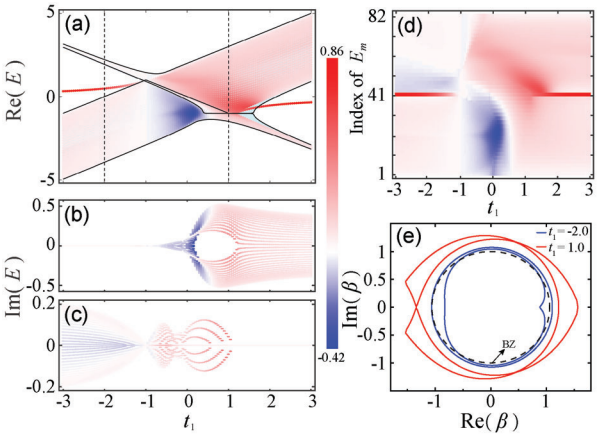

Figure 5. a–c) The real and imaginary parts of eigen-energy spectra under OBC as a function of $t_1 \in [-3, 3]$ in models including the long-range hopping amplitudes. The cyan regime with the black lines labels the real eigen-energy spectra under PBC in (a). d) The dIPR distributions of total eigen-energy spectra under the OBC for the lattice with $N = 41$. e) The GBZs under OBC for the lattice with $N = 41$ at $t_1 = -2.0$ and 1.0. The parameters are chosen to be $t_2 = 1.0$, $t_3 = t_4 = 0.5$, $\Delta_1 = \Delta_2 = 0.3$.

plot the GBZs in Figure 4d. In the model here with $t_3 \neq 0$, there are two closed loops for each choice of t_1. Specially, for $t_1 = 0.2$, the GBZ consists one loop less than the unit circle and the other loop greater than the unit circle, consistent with the dIPR shown in Figure 4a–c that there exists the right localized NHSE associated with the upper spectra and the left localized NHSE associated with the lower spectra. As for $t_1 = 1.0$, both loops are larger than the unit circle, corresponding to the right localized NHSE. We also note that, if we include $\Delta_2 \neq 0$ in addition to $t_3 \neq 0$, the spectra similar to those in Figure 3 can be found, and the physics is therefore similar when the chiral symmetry of the lattice is broken.

5. Study Model with Double Long-Range Hopping Amplitudes

As the last example, we consider the case with both next-nearest-neighbor hopping amplitudes included, that is, $t_3 \neq 0$ and $t_4 \neq 0$. Such lattice is also referred as the Zigzag lattice[80,81] with the chiral symmetry broken. The Hamiltonian in the k space becomes

$$\mathcal{H}(k) = \begin{bmatrix} 2t_3 \cos k & (t_1 + \Delta_1)e^{-ik} + (t_2 - \Delta_2) \\ (t_1 - \Delta_1)e^{ik} + (t_2 + \Delta_2) & 2t_4 \cos k \end{bmatrix} \quad (11)$$

where both diagonal terms are non-zeros, so the corresponding eigen-energy spectra are

$$\begin{aligned} E_{\pm}(k) &= (t_3 + t_4)\cos k \pm \sqrt{(t_3 + t_4)^2 \cos^2 k + \left[(t_1 - \Delta_1)e^{ik} + (t_2 + \Delta_2)\right]\left[(t_1 + \Delta_1)e^{-ik} + (t_2 - \Delta_2)\right]} \\ &= (t_3 + t_4)\cos k \pm \sqrt{(t_3 + t_4)^2 \cos^2 k + {t_1}^2 + {t_2}^2 - (\Delta_1^2 + \Delta_2^2) + 2(t_1 t_2 + \Delta_1 \Delta_2)\cos k - i2(t_1 \Delta_2 + \Delta_1 t_2)\sin k} \end{aligned} \quad (12)$$

The square root in Equation 12 indicates that the transition point of NHSE is strongly dependent on the term $t_1\Delta_2 + \Delta_1 t_2$.

We plot the eigen-energy spectra with dIPR in **Figure 5**a–c. One can see that the edge states on both sides in the energy gap are localized at the right boundary in Figure 5a. As for the bulk spectra, there is a distinct transition area of NHSE at $t_1 = -1.0$. It actually elucidates that $t_1\Delta_2 + \Delta_1 t_2 = 0$ results in the eigen-energy spectra $E(k) \in \mathcal{R}$ under PBC, which leads to no interior space in the complex plane, and overlapping with ones under OBC. In Figure 5a, we notice that the upper left real spectra are narrow and each dIPR approaches zero. This implies that complicated changes in NHSE occur and rich variations of spectra exhibit. In particular, from Figure 5b,c, we can see that the narrow upper left real spectra in Figure 5a contain distinctive localized features.

To explicitly show the total localization features and clearly catch the changes of NHSE, we further plot the dIPR distributions with all indices of eigen-energy spectra in Figure 5d. One can see the appearance of two changes of NHSE in the regime of $-3 < t_1 < -1$, which are different from results in previous sections. One can understand such phenomena from Equation 12, which shows terms with and without the square root interact for the same k and results in the crossing of the eigen-energy spectra. (We also provide more analyses in **Figure 6**a,b in the following).

Meanwhile, we also follow the standard approach to calculate the GBZs for $t_1 = 1.0$ and $t_1 = -2.0$, respectively, which satisfies

$$\begin{aligned} &-t_3 t_4 \beta^4 + \left[(t_1 - \Delta_1)(t_2 - \Delta_2) + (t_3 + t_4)E\right]\beta^3 \\ &+ \left[{t_1}^2 + {t_2}^2 - 2t_3 t_4 - (\Delta_1^2 + \Delta_2^2) - E^2\right]\beta^2 \\ &+ \left[(t_1 + \Delta_1)(t_2 + \Delta_2) + (t_3 + t_4)E\right]\beta - t_3 t_4 = 0 \end{aligned} \quad (13)$$

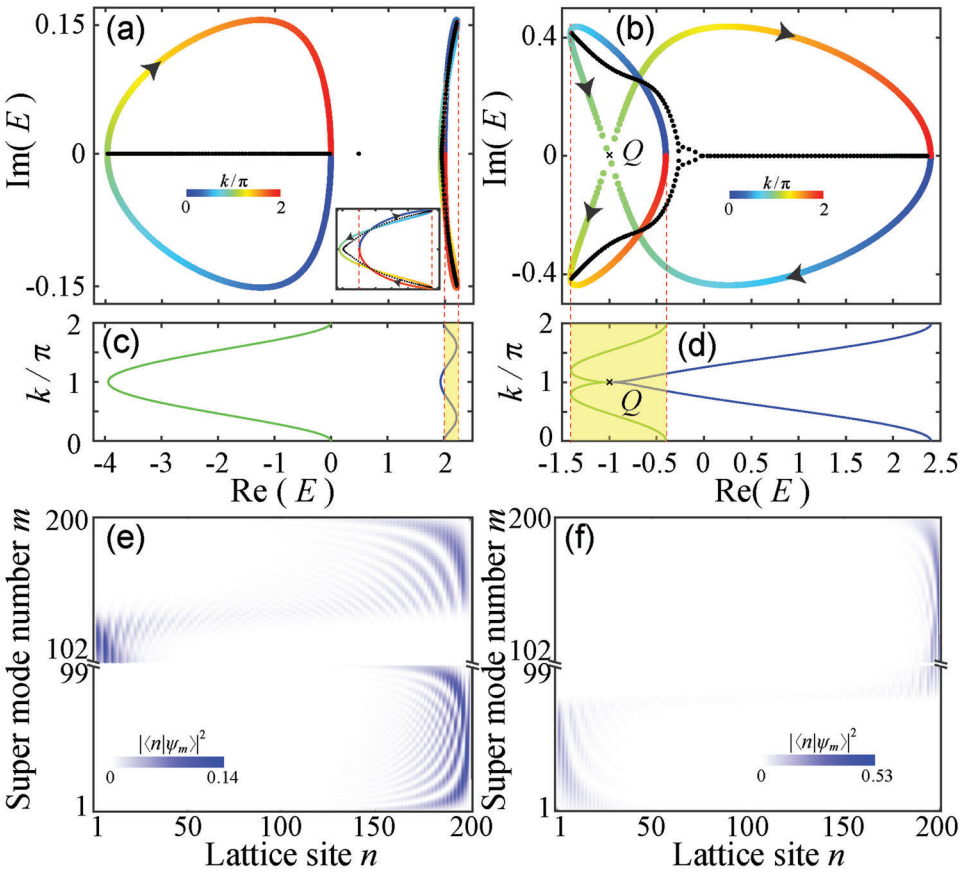

Figure 6. a,b) The eigen-energy spectra under PBCs (colored dots) and OBC (black dots) in the complex plane while the real spectra of the right and left parts are shown in c,d), respectively. The arrows represent the evoluted directions along $k \in [0, 2\pi)$ under PBC. Inset: A zoom-in for the right part of the spectra. e) and f) The distributions of bulk states corresponding to (a) and (b). The parameters are chosen to be $t_1 = -2$ for (a), $t_1 = 0.4$ for (b), with $t_3 = t_4 = 0.5$, and $\Delta_1 = \Delta_2 = 0.3$.

Due to double long-range hopping amplitudes, Equation 8 of the GBZ is changed into a quartic equation. The solutions have four roots $|\beta_1| \leqslant |\beta_2| \leqslant |\beta_3| \leqslant |\beta_4|$ but reserve two terms $|\beta_2| = |\beta_3|$ to obey in the thermodynamic limit at $N \to \infty$.[19,20] We plot GBZs for two cases to exhibit the localized property in Figure 5e. For $t_1 = -2.0$, the GBZ consists of two closed curves with one outside the unit circle and the other intersected by the BZ, implying two changes of NHSE in Figure 5d, whereas for $t_1 = 1.0$, the GBZs are both outside the unit circle, which are consistent with dIPR distributions in Figure 5a–d. Interestingly, it is the intersection of spectra under PBC that leads to more than one change in localizations of NHSE and we will explore details in the following with the aid of the topological winding number.

We here choose parameters $t_1 = -2.0$ and 0.4, and plot the eigen-energy spectra under PBC and OBC in Figure 6a,b respectively. For the case of $t_1 = -2.0$, the left part of the spectra in Figure 6a evolves clockwise with the increasing k, which corresponds to $w(E) = +1$ and the NHSE localized at the right boundary. However, the right part of the spectra forms a closed loop with crossings under PBC, which appears to be an arc shape. From the real spectra in Figure 6c, one can see this crossing manifests in the values for a fixed eigen-energy. Or in other words, for each eigen-energy value falling into the yellow shadow in Figure 6c, there are four solutions $k_1 \leqslant k_2 \leqslant k_3 \leqslant k_4$ accompanied with the winding as shown in Figure 6a. Hence one can see the change of NHSE localized at different boundaries near the 100*th* super mode in Figure 6e. As for the change of NHSE in the vicinity of the 100*th* super mode, one can understand it from different winding directions in two parts of the spectra in Figure 6a. For the case of $t_1 = 0.4$, different features of spectra and NHSE are found in Figure 5 as the parameter t_1 falls in different regimes. We can also see similar crossing characteristics in spectra shown in Figure 6b,d. Here, the crossing point labeled as Q in Figure 6b satisfies $E_+(\pi) = E_-(\pi)$ in Equation 12. The yellow shadow in Figure 6d also reflects the change of NHSE in Figure 6f from the solutions for a fixed real eigen-energy. From all above examples, one can see that it is possible to acquire the transition and change of NHSE for localized features from the (real) eigen-energy spectra. Note that if we further increase t_1, the spectra under PBC separate into two parts near the crossing point Q and the winding of the left part reverses into the clockwise direction at $t_1 \approx 0.6$, which corresponds to the dIPR distributed on the right boundary for NHSE in Figure 5a.

6. Conclusion

In conclusion, we explore a Zigzag lattice without/with long-range hopping amplitudes that may or may not possess a chiral symmetry correspondingly. Transitions of NHSE are studied from the eigen-energy spectra obtained under PBC together with dIPR obtained under the OBC. Without long-range hopping amplitudes, the model Hamiltonian satisfies chiral symmetry such that the spectra are symmetrical, and the transitions of NHSE occur when the closed eigen-energy spectra under PBC have no interior where the widths of real spectra under PBC measured along the real axis $\mathrm{Im}(E)=0$ is vanishing or the imaginary parts under the square root in Equation 3 approach zero. The criteria for the transitions still hold with single and double long-range hopping amplitudes respectively in spite of the invalidation of chiral symmetry, thus it offers a convenient avenue to take the link between the eigen-energy spectra and NHSE. Our proposed lattice is general and can be realized in various platforms in either spatially-arranged resonators or artificial lattices with synthetic dimensions[78–88] under current photonic technologies. Here, we introduce the non-Hermitian Hamiltonian with nonreciprocal hopping amplitudes in the semiclassical regime. By considering quantum jumps, one could further explore exceptional points of non-Hermitian Hamiltonians and Liouvillians in the quantum regime.[89,90] Our work unveils the important correspondence between the NHSE and the eigen-energy spectra, and hence paves the way for investigating exotic non-Hermitian physical phenomena and manipulating NHSE in complicated lattice models.

We noticed an accepted paper[91] when our manuscript was in the production stage.

Acknowledgements

This research was supported by the National Natural Science Foundation of China (12122407, 11974245, 11974075, and 12204304) and the Shanghai Municipal Science and Technology Major Project (2019SHZDZX01-ZX06). L.Y. thanks the sponsorship from Yangyang Development Fund and the support from the Program for Professor of Special Appointment (Eastern Scholar) at Shanghai Institutions of Higher Learning.

Conflict of Interest

The authors declare no conflict of interest.

Data Availability Statement

The data that support the findings of this study are available from the corresponding author upon reasonable request.

Keywords

bulk-boundary correspondence, chiral symmetry, general Brillouin zone, non-Hermitian skin effect, transition point, zigzag lattices

Received: January 16, 2023
Revised: March 21, 2023
Published online: April 22, 2023

[1] M. Z. Hasan, C. L. Kane, *Rev. Mod. Phys.* **2010**, *82*, 3045.
[2] X.-L. Qi, S.-C. Zhang, *Rev. Mod. Phys.* **2011**, *83*, 1057.
[3] A. Bansil, H. Lin, T. Das, *Rev. Mod. Phys.* **2016**, *88*, 021004.
[4] C.-K. Chiu, J. C. Y. Teo, A. P. Schnyder, S. Ryu, *Rev. Mod. Phys.* **2016**, *88*, 035005.
[5] S.-Q. Shen, *Topological Insulators*, 2nd Ed., Springer, Singapore **2017**.
[6] N. R. Cooper, J. Dalibard, I. B. Spielman, *Rev. Mod. Phys.* **2019**, *91*, 015005.
[7] R. El-Ganainy, K. G. Makris, M. Khajavikhan, Z. H. Musslimani, S. Rotter, D. N. Christodoulides, *Nat. Phys.* **2018**, *14*, 11.
[8] K. Yokomizo, S. Murakami, *Phys. Rev. Research* **2020**, *2*, 043045.
[9] Y. Ashida, Z. Gong, M. Ueda, *Adv. Phys.* **2020**, *69*, 249.
[10] M. V. Hosseini, M. Askari, *Sci. Rep.* **2021**, *11*, 22206.
[11] Y. Cao, Y. Li, X. Yang, *Phys. Rev. B* **2021**, *103*, 075126.
[12] W. Wang, X. Wang, G. Ma, *Nature* **2022**, *608*, 50.
[13] L. Feng, R. El-Ganainy, L. Ge, *Nat. Photonics* **2017**, *11*, 752.
[14] H. Jiang, C. Yang, S. Chen, *Phys. Rev. A* **2018**, *98*, 052116.
[15] S. Longhi, *Ann. Phys.* **2018**, *530*, 1800023.
[16] F. K. Kunst, E. Edvardsson, J. C. Budich, E. J. Bergholtz, *Phys. Rev. Lett.* **2018**, *121*, 026808.
[17] Q. Zhong, M. Khajavikhan, D. N. Christodoulides, R. El-Ganainy, *Nat. Commun.* **2018**, *9*, 4808.
[18] S. Yao, F. Song, Z. Wang, *Phys. Rev. Lett.* **2018**, *121*, 136802.
[19] S. Yao, Z. Wang, *Phys. Rev. Lett.* **2018**, *121*, 086803.
[20] K. Yokomizo, S. Murakami, *Phys. Rev. Lett.* **2019**, *123*, 066404.
[21] F. Song, S. Yao, Z. Wang, *Phys. Rev. Lett.* **2019**, *123*, 246801.
[22] K. Kawabata, K. Shiozaki, M. Ueda, M. Sato, *Phys. Rev. X* **2019**, *9*, 041015.
[23] N. Okuma, K. Kawabata, K. Shiozaki, M. Sato, *Phys. Rev. Lett.* **2020**, *124*, 086801.
[24] L. Xiao, T. Deng, K. Wang, G. Zhu, Z. Wang, W. Yi, P. Xue, *Nat. Phys.* **2020**, *16*, 761.
[25] Z. Yang, K. Zhang, C. Fang, J. Hu, *Phys. Rev. Lett.* **2020**, *125*, 226402.
[26] K. Yokomizo, S. Murakami, *Phys. Rev. Research* **2020**, *2*, 043045.
[27] E. J. Bergholtz, J. C. Budich, F. K. Kunst, *Rev. Mod. Phys.* **2021**, *93*, 015005.
[28] L. Xiao, T. Deng, K. Wang, Z. Wang, W. Yi, P. Xue, *Phys. Rev. Lett.* **2021**, *126*, 230402.
[29] W.-T. Xue, Y.-M. Hu, F. Song, Z. Wang, *Phys. Rev. Lett.* **2022**, *128*, 120401.
[30] D. Cheng, B. Peng, M. Xiao, X. Chen, L. Yuan, S. Fan, *Phys. Rev. B* **2022**, *105*, L201105.
[31] C. Hou, L. Li, S. Chen, Y. Liu, L. Yuan, Y. Zhang, Z. Ni, *Phys. Rev. Research* **2022**, *4*, 043222.
[32] S. Longhi, *Phys. Rev. Lett.* **2022**, *128*, 157601.
[33] T. Ozawa, H. M. Price, A. Amo, N. Goldman, M. Hafezi, L. Lu, M. C. Rechtsman, D. Schuster, J. Simon, O. Zilberberg, I. Carusotto, *Rev. Mod. Phys.* **2019**, *91*, 015006.
[34] S. Longhi, *Opt. Lett.* **2022**, *47*, 2040.
[35] J. Jiang, B. Yan, Y. Peng, J. Xie, A. Shi, J. Liu, *Opt. Lett.* **2022**, *47*, 437.
[36] G. Ma, M. Xiao, C. Chan, *Nat. Rev. Phys.* **2019**, *1*, 281.
[37] G. Ananya, B. Martin, v. W. Jasper, C. Corentin, *Proc. Natl. Acad. Sci.* **2020**, *117*, 29561.
[38] W. Wang, X. Wang, G. Ma, *Nature* **2022**, *608*, 50.
[39] K. Luo, R. Yu, H. Weng, *Research* **2018**, *2018*, 6793752.
[40] M. Ezawa, *Phys. Rev. B* **2019**, *100*, 081401.
[41] T. Helbig, T. Hofmann, S. Imhof, M. Abdelghany, T. Kiessling, L. W. Molenkamp, C. H. Lee, A. Szameit, M. Greiter, R. Thomale, *Nat. Phys.* **2020**, *16*, 747.
[42] S. Liu, R. Shao, S. Ma, L. Zhang, O. You, H. Wu, Y. J. Xiang, T. J. Cui, S. Zhang, *Research* **2021**, *2021*, 5608038.
[43] W. Zhu, X. Fang, D. Li, Y. Sun, Y. Li, Y.and Jing, H. Chen, *Phys. Rev. Lett.* **2018**, *121*, 124501.

[44] H. Gao, H. Xue, Z. Gu, T. Liu, J. Zhu, B. Zhang, *Nat. Commun.* **2021**, *12*, 1888.
[45] L. Zhang, Y. Yang, Y. Ge, Y. J. Guan, Q. Chen, Q. Yan, F. Chen, R. Xi, Y. Li, D. Jia, S. Q. Yuan, H. X. Sun, H. Chen, B. Zhang, *Nat. Commun.* **2021**, *12*, 6297.
[46] X. Wen, X. Zhu, A. Fan, W. Y. Tam, J. Zhu, H. W. Wu, F. Lemoult, M. Fink, J. Li, *Commun. Phys.* **2022**, *5*, 18.
[47] Z. Gong, Y. Ashida, K. Kawabata, K. Takasan, S. Higashikawa, M. Ueda, *Phys. Rev. X* **2018**, *8*, 031079.
[48] K. Yamamoto, M. Nakagawa, K. Adachi, K. Takasan, M. Ueda, N. Kawakami, *Phys. Rev. Lett.* **2019**, *123*, 123601.
[49] W. B. Rui, Z. Zheng, C. Wang, Z. D. Wang, *Phys. Rev. Lett.* **2022**, *128*, 226401.
[50] C. M. Bender, S. Boettcher, *Phys. Rev. Lett.* **1998**, *80*, 5243.
[51] P. Ambichl, K. G. Makris, L. Ge, Y. Chong, A. D. Stone, S. Rotter, *Phys. Rev. X* **2013**, *3*, 041030.
[52] E. F. F. T. Luis, *J. Phys. Mater.* **2019**, *3*, 014002.
[53] B. Dóra, D. Sticlet, C. Moca, *Phys. Rev. Lett.* **2022**, *128*, 146804.
[54] S. K. Özdemir, S. Rotter, F. Nori, L. Yang, *Nat. Mater.* **2019**, *18*, 783.
[55] M.-A. Miri, A. Alù, *Science* **2019**, *363*, eaar7709.
[56] M. Parto, Y. G. Liu, B. Bahari, M. Khajavikhan, D. N. Christodoulides, *Nanophotonics* **2020**, *10*, 403.
[57] K. Ding, C. Fang, G. Ma, *Nat. Rev. Phys.* **2022**, *4*, 745.
[58] H. Nasari, G. G. Pyrialakos, D. N. Christodoulides, M. Khajavikhan, *Opt. Mater. Express* **2023**, *13*, 870.
[59] T. Gao, E. Estrecho, K. Y. Bliokh, T. C. H. Liew, M. D. Fraser, S. Brodbeck, M. Kamp, C. Schneider, S. Höfling, Y. Yamamoto, F. Nori, Y. S. Kivshar, A. G. Truscott, R. G. Dall, E. A. Ostrovskaya, *Nature* **2015**, *526*, 554.
[60] S. Assawaworrarit, S. Fan, *Nat. Electron.* **2020**, *3*, 273.
[61] S. Longhi, D. Gatti, G. Della Valle, *Sci. Rep.* **2015**, *5*, 13376.
[62] S. Longhi, *Opt. Lett.* **2015**, *40*, 5694.
[63] F. Song, S. Yao, Z. Wang, *Phys. Rev. Lett.* **2019**, *123*, 170401.
[64] W.-T. Xue, M.-R. Li, Y.-M. Hu, F. Song, Z. Wang, *Phys. Rev. B* **2021**, *103*, L241408.
[65] J. del Pino, J. J. Slim, E. Verhagen, *Nature* **2022**, *606*, 82.
[66] N. Hatano, D. R. Nelson, *Phys. Rev. Lett.* **1996**, *77*, 570.
[67] N. Hatano, D. R. Nelson, *Phys. Rev. B* **1997**, *56*, 8651.
[68] T. E. Lee, *Phys. Rev. Lett.* **2016**, *116*, 133903.
[69] V. M. Martinez Alvarez, J. E. Barrios Vargas, L. E. F. Foa Torres, *Phys. Rev. B* **2018**, *97*, 121401.
[70] Y. Xiong, *J. Phys. Commun.* **2018**, *2*, 035043.
[71] X. Zhang, T. Zhang, M.-H. Lu, Y.-F. Chen, *Adv. Phys.: X* **2022**, *7*, 2109431.
[72] O. Nobuyuki, S. Masatoshi, *Annu. Rev. Conden. Ma. P.* **2023**, *14*, 83.
[73] K. Zhang, Z. Yang, C. Fang, *Phys. Rev. Lett.* **2020**, *125*, 126402.
[74] W. P. Su, J. R. Schrieffer, A. J. Heeger, *Phys. Rev. Lett.* **1979**, *42*, 1698.
[75] W. P. Su, J. R. Schrieffer, A. J. Heeger, *Phys. Rev. B* **1980**, *22*, 2099.
[76] Q.-B. Zeng, R. Lü, *Phys. Rev. B* **2022**, *105*, 245407.
[77] W. Deng, T. Chen, X. Zhang, *Phys. Rev. Research* **2022**, *4*, 033109.
[78] Z. Lin, L. Ding, S. Ke, X. Li, *Opt. Lett.* **2021**, *46*, 3512.
[79] K. Wang, A. Dutt, C. C. Wojcik, S. Fan, *Nature* **2021**, *598*, 59.
[80] F. A. An, E. J. Meier, B. Gadway, *Phys. Rev. X* **2018**, *8*, 031045.
[81] H. Cai, J. Liu, J. Wu, Y. He, S. Zhu, J.-X. Zhang, D.-W. Wang, *Phys. Rev. Lett.* **2019**, *122*, 023601.
[82] L. Yuan, M. Xiao, Q. Lin, S. Fan, *Phys. Rev. B* **2018**, *97*, 104105.
[83] S. Weidemann, M. Kremer, T. Helbig, T. Hofmann, A. Stegmaier, M. Greiter, R. Thomale, A. Szameit, *Science* **2020**, *368*, 311.
[84] D. Yu, B. Peng, X. Chen, X.-J. Liu, L. Yuan, *Light: Sci. Appl.* **2021**, *10*, 209.
[85] G. Li, L. Wang, R. Ye, S. Liu, Y. Zheng, L. Yuan, X. Chen, *Adv. Photonics* **2022**, *4*, 036002.
[86] Q. Lin, T. Li, L. Xiao, K. Wang, W. Yi, P. Xue, *Phys. Rev. Lett.* **2022**, *129*, 113601.
[87] Z. Gong, M. Bello, D. Malz, F. K. Kunst, *Phys. Rev. A* **2022**, *106*, 053517.
[88] K. Ding, C. Fang, G. Ma, *Nat. Rev. Phys.* **2022**, *4*, 745.
[89] F. Minganti, A. Miranowicz, R. W. Chhajlany, F. Nori, *Phys. Rev. A* **2019**, *100*, 062131.
[90] F. Minganti, A. Miranowicz, R. W. Chhajlany, I. I. Arkhipov, F. Nori, *Phys. Rev. A* **2020**, *101*, 062112.
[91] W.-H. Zhou, C.-X. Zhang, *Phys. Scr.* **2023**, *98*, 055202.